An improved three-dimensional two-temperature model for multi-pulse femtosecond laser ablation of aluminum

Jinping Zhang, Yuping Chen, Mengning Hu, and Xianfeng Chen

Citation: Journal of Applied Physics **117**, 063104 (2015); doi: 10.1063/1.4907990
View online: http://dx.doi.org/10.1063/1.4907990
View Table of Contents: http://scitation.aip.org/content/aip/journal/jap/117/6?ver=pdfcov
Published by the AIP Publishing

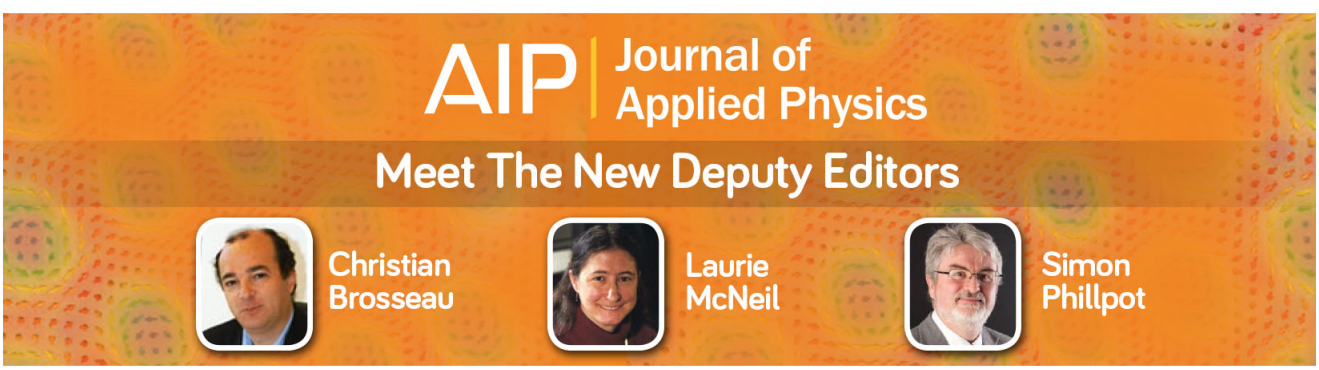

An improved three-dimensional two-temperature model for multi-pulse femtosecond laser ablation of aluminum

Jinping Zhang, Yuping Chen,[a] Mengning Hu, and Xianfeng Chen
State Key Laboratory of Advanced Optical Communication Systems and Networks, Department of Physics and Astronomy, Shanghai Jiao Tong University, Shanghai 200240, China

(Received 30 October 2014; accepted 30 January 2015; published online 10 February 2015)

In this paper, an improved three-dimensional two-temperature model for multi-pulse femtosecond laser ablation of aluminum was proposed and proved in our experiment. Aiming to achieve hole-drilling with a high ratio of depth/entrance diameter in vacuum, this model can predict the depth and radius of the drilled holes precisely when employing different laser parameters. Additionally, for multi-pulse laser ablation, we found that the laser fluence and number of pulses are the dominant parameters and the multi-pulse ablation threshold is much lower than the single-pulse one, which will help to obtain high-quality holes. © *2015 AIP Publishing LLC*.
[http://dx.doi.org/10.1063/1.4907990]

I. INTRODUCTION

In the last two decades, ultrashort-pulsed laser interactions with metals have attracted great interests, because processing metals by femtosecond lasers has the advantages of rapid energy deposition and reducing the size of the undesirable heat-affected zone.[1–11] Various theoretical studies such as phase explosion,[12] Coulomb explosion,[13] and thermoelastic-wave effects[14] have been proposed to explain ultrashort-pulsed laser ablation. Du *et al*. explained that the dominant mechanism consists of three stages, including the absorption of laser energy through photon-electron coupling, energy distribution to the lattice through electron-phonon coupling, and normal energy diffusion into the material through phonon-phonon collision.[15] It has been accepted that the electron-phonon coupling (i.e., two temperature relaxation) plays an important role in processing metallic targets under the irradiation of the ultrashort laser pulses in the ablation regime.[16] Typically, the electron-lattice relaxation timescale is of several picoseconds, and the laser pulse has a shorter duration of several hundred femtoseconds. The material is excited into a highly non-equilibrium state when exposed to sub-picosecond laser pulses.[2]

A two-temperature model (TTM) has been employed for solving ultrashort laser processing of metals. This continuous model describes the energy transfer inside a metal with two coupled generalized heat conduction equations for the temperatures of the electrons and the phonons (lattice). Heating in thin metal films using a single femtosecond laser pulse has been reported theoretically and experimentally. Sonntag *et al*. proposed a hybrid model which combines the classic two-temperature model and the molecular dynamics to observe the actual ablation process on atomistic scales.[17] In our previous work, Li *et al*. presented simulated three-dimensional (3D) ablation craters which irradiated by a single pulse with different energies.[18] Nevertheless, the underlying energy transport mechanism for multi-pulse femtosecond laser heating remains poorly understood. Moreover, researchers have widely used the TTM to clarify the electron-phonon energy transfer characteristics of thin metal films.[18–22] In most studies, the spot size of a Gaussian beam w has been assumed to be a constant for the sake of simplicity. However, this assumption may yield inaccurate results for ablation of thick films by multi-pulse lasers, especially for drilling micron-scale holes with a high aspect ratio, e.g., 10:1, where the spot size of the Gaussian beam varies substantially with the depth. Thus, an improved model is needed to analyze energy transfer inside a thick film by multi-pulse femtosecond laser ablation.

In this paper, by employing an improved 3D TTM, we numerically and experimentally demonstrate the heat flux equations in aluminum film target exposed to multi-pulse femtosecond laser. For drilling high-aspect-ratio holes, the beam spot size w_0 replaced by $w(z)$ with the axial position z, which describes the laser beam propagation more accurately. Then an improved simulated 3D full temperature field picture of multi-pulse ablation is obtained with the finite element method (FEM), and the simulation results are generally in good agreement with the experimental data. The influences of the laser parameters such as laser fluence, number of pulses, and beam waist w_0 are carefully analyzed in the latter discussions.

II. IMPROVED 3D TWO-TEMPERATURE MODEL FOR MULTI-PULSE LASER ABLATION

In our previous model,[18] the single femtosecond laser pulse ablation process has been studied by TTM in thin aluminum films. However, for high-aspect-ratio holes drilled in thick metal films, the mechanism of single-pulse laser ablation does not work and cannot provide useful data for us, then an improved 3D TTM should be employed to calculate the multi-pulse femtosecond laser ablation. The corresponding interpretation is as follow: After 5 ps for each single pulse laser ablation, the electron and lattice temperatures are approximately the same and the target keeps the state of

[a]Electronic mail: ypchen@sjtu.edu.cn

thermal equilibrium, which means that the main material removal occurs on a timescale of a few ps.[18,23] The repetition rate of the laser is 1 kHz, and the time between each pulse is 1 ms which is quite larger than the thermal equilibrium time of 5 ps. As a result, for multi-pulse laser simulations, we can assume that material removal is independent for each single-pulse laser ablation. Therefore, the TTM is suitable for multi-pulse laser ablation and needed to be combined with finite-difference method (FDM) to investigate the ablation mechanism in thick samples.

The TTM has been proposed to describe the laser energy transfer inside a metal plate with two coupled nonlinear differential equations[2]

$$C_e\frac{\partial T_e}{\partial t}=k_e\left(\frac{\partial^2 T_e}{\partial x^2}+\frac{\partial^2 T_e}{\partial y^2}+\frac{\partial^2 T_e}{\partial z^2}\right)-g(T_e-T_l)+Q(x,y,z,t), \tag{1}$$

$$C_l\frac{\partial T_l}{\partial t}=g(T_e-T_l), \tag{2}$$

where the subscripts e and l refer to the electron and lattice parameters, $C_e=\gamma T_e$ and k_e are the heat capacity and thermal conductivity of electron, C_l is the lattice heat capacity which can be considered as a constant, the electron-phonon coupling g is dependent on the temperature, which has been explicitly analyzed by Lin *et al.*[24] To simplify Eqs. (1) and (2), we set $g=5.69\times10^{17}$ J/(m^3 K s) as a constant.[17]

The 3D energy absorption rate Q is presented by[10,25]

$$Q(x,y,z,t)=S(x,y,z)\cdot T(t), \tag{3}$$

where

$$S(x,y,z)=\frac{1-R}{\delta+\delta_b}\cdot F\times\exp\left(-\frac{z-z_s}{\delta+\delta_b}-\frac{2(x-x_0)^2+2(y-y_0)^2}{w_0^2}\right), \tag{4}$$

$$T(t)=\frac{1}{t_p}\sqrt{\frac{4\ln 2}{\pi}}\exp\left(-4\ln 2\left(\frac{t-2t_p}{t_p}\right)^2\right). \tag{5}$$

Laser absorption from the surface into the bulk metal follows Lambert-Beers law, where R is the reflectance of the target, δ is the optical penetration of aluminum film, and δ_b is the ballistic length. The laser pulse is a Gaussian distribution both in time and space, F is the average laser fluence, x_0 and y_0 are the x-coordinate and y-coordinate of the laser spot center, w_0 is 1/e radius of the laser spot, and t_p is the full width at half maximum (FWHM) pulse duration, respectively. The laser absorption into the work piece begins at $z=0$. For multi-pulse laser ablation, the local target surface position z_s will decrease due to the material removal after each laser pulse ablation. z_s is a function of x and y.

For high-aspect-ratio holes drilling in 100-μm-thick aluminum film, e.g., 10:1, the thickness of the sheet is larger than the Rayleigh range Z_R

$$Z_R=\frac{n\pi w_0^2}{\lambda}. \tag{6}$$

For example, a laser with the laser wavelength $\lambda=800$ nm, the refractive index $n=1$, and the beam waist $w_0=4.5$ μm yields $Z_R\sim90$ μm. Beam spot size w is a function of axial position z, and it is characterized[26]

$$w(z)=w_0\left(1+\frac{z^2}{Z_R^2}\right)^{1/2}. \tag{7}$$

To account for the small spatial extent after laser drilling, a two-temperature model is presented in which the incident laser power becomes position dependent (Fig. 1(b)). Notice that the spatial propagation of the laser pulse in the previous model[18–22] (Fig. 1(a)) is neglected. Thus, the laser intensity takes the form

$$S(x,y,z)=\frac{1-R}{\delta+\delta_b}\cdot F\cdot\frac{w_0^2}{w^2(z)}\times\exp\left(-\frac{z-z_s}{\delta+\delta_b}-\frac{2(x-x_0)^2+2(y-y_0)^2}{w^2(z)}\right). \tag{8}$$

Compared with Eq. (4), w_0 is replaced by $w(z)$, which becomes suitable for the multi-pulse laser ablation.

In our latter simulations of laser ablation, we use the finite-difference method to solve Eqs. (1) and (2). The simulation starts at time $t=0$, and the initial conditions for both electrons and lattice are fixed at room temperature. As the ablation process takes place during the femtosecond-to-picosecond time period, it is reasonable to assume that heat losses from the metal film to the surrounding can be ignored. Therefore, the initial and boundary conditions can be described by

$$T_e(x,y,z,t=0)=T_l(x,y,z,t=0)=300\,\text{K}, \tag{9}$$

$$\left.\frac{\partial T_e}{\partial n}\right|_\Omega=\left.\frac{\partial T_l}{\partial n}\right|_\Omega=0, \tag{10}$$

where Ω represents the six boundary surfaces of the 3D aluminum film. The computational area has the dimension

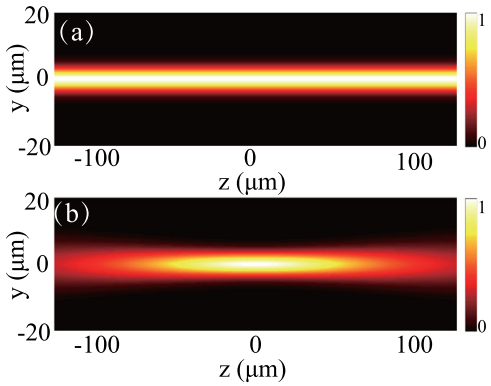

FIG. 1. Comparison of the intensity of laser beam propagation in the focal region. (a) Laser intensity propagation in the previous model. (b) Revised position-dependent intensity of focal region.

of $100\,\mu m \times 100\,\mu m \times 100\,\mu m$. The other parameters are given as follows:[17] $k_e = 235\,J/(m\,K\,s)$, $\gamma = 134.5\,J/(m^3\,K^2)$, $g = 5.69 \times 10^{17}\,J/(m^3\,K\,s)$, $C_l = 2.42 \times 10^6\,J/(m^3\,K)$, $R = 0.88$, $\delta = 20\,nm$, $\delta_b = 100\,nm$, $T_0 = 300\,K$, $t_p = 100\,fs$, and $\lambda = 800\,nm$.

During the above calculation of the ablation process, we suppose that the material will be removed if the temperature of the lattice is higher than the thermodynamic critical temperature of aluminum (5720 K),[27] because the extremely high pressure in the ablated region will be released through the adiabatic expansion.[12]

III. RESULTS AND DISCUSSION

In our experiments, a commercial femtosecond Ti:Sapphire laser system with repetition rate of 1 kHz is used to drill holes. This laser system is able to provide 1 mJ, 100 fs laser pulse at the wavelength of 800 nm, and the target material is a 100-μm-thick aluminum film. An aperture and a rotatable half-wave plate are used to optimize the shape of the laser spot and change the energy of the laser pulses. A desired number of pulses can be controlled by a speed-controllable mechanical shutter. The beam is finally focused into the sample using a 20× objective lens. The sample is fixed onto a motor-controlled XYZ stage with a resolution of 0.4 μm, and the incident laser beam irradiates the sample perpendicularly. A CCD camera is used to monitor the ablation process.

The SEM images of drilling-through hole entrances at different laser fluences with 1 and 3 J/cm^2 are shown in Fig. 2. The hole diameter is about 10 μm in Fig. 2(a) while 12 μm in Fig. 2(b). It is shown that the cracks and recasting melt extend over a larger region as the laser fluence increasing. Notice that the hole diameter does not increase much with the increase of the laser fluence, however, the thermal damage is more obvious. It has been accepted that drilling holes with relative lower laser fluence serves to reduce the recasting melt and obtain more clean open up hole entrance. Thus, determination of the multi-pulse ablation threshold is important for drilling holes.

The ablation threshold of aluminum has been predicted in previous report[18] by $D^2 = 2w_0^2 \ln(F_0/F_{th})$, where F_0 represents the incident laser fluence, F_{th} is the single pulse ablation threshold, and D is the crater diameter. In this paper, we recalculate the multi-pulse ablation threshold by using the logarithmic dependence of the ablation rate on the laser fluence. Ablation rates are calculated from the depth of craters

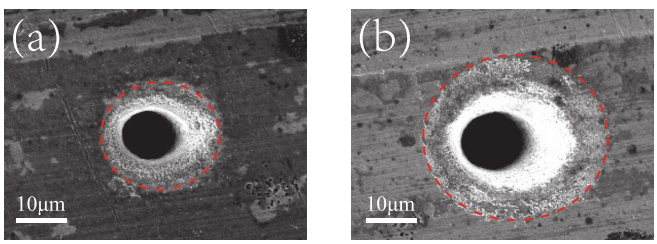

FIG. 2. SEM images of drilling-through hole entrances formed by static focus at the front surface with different laser fluence and number of pulses in vacuum. (a) $F = 1\,J/cm^2$, $N = 1100$; (b) $F = 3\,J/cm^2$, $N = 500$.

produced by multi-pulse laser which is incident normally onto the sample surface. For the calculation of the multi-pulse ablation threshold, we can use the depth of single-pulse ablation craters which is measured by an atomic force microscope (AFM). Generally, the laser fluence employed is larger than the threshold; therefore, we can replace the ablation rate d by the depth of single-pulse ablation h_a.[28] Thus

$$h_a = \alpha_{eff}^{-1} \ln\left(\frac{F_0^{av}}{F_{th}^{N>1}}\right), \tag{11}$$

where α_{eff}^{-1} can be interpreted as the effective optical penetration depth.

Fig. 3 shows this linear relationship between the ablation rate and the logarithm of laser fluence. By extrapolating the fitted line to zero, we can obtain a multi-pulse ablation threshold of $F_{th}^{N>1} = 0.52 \pm 0.01\,J/cm^2$. We also find that the multi-pulse threshold is smaller than the single-pulse threshold[18] $F_{th}^{N=1} = 0.9\,J/cm^2$ due to the incubation effect.[29] Therefore, the multi-pulse ablation threshold is expected in our experiment.

Moreover, we also investigate the effect of other laser parameters, such as the laser fluence, the number of pulses, and the beam waist. The TTM equations are solved using FEM by varying laser parameters. The initial and boundary conditions are referred in Part II. The simulation results are shown in Fig. 4. We present three simulated 3D ablation craters with certain number of pulses $N = 50$ but different laser fluences: 2, 4, and 6 J/cm^2. The cross-sectional profiles at the centerline of the craters are plotted in Fig. 4(d). As shown in Fig. 4(d), both widening and deepening of the craters appear for increasing laser fluences, while the depth of the craters increases more quickly.

The simulated ablation craters with different numbers of pulses are shown in Fig. 5. From Fig. 5(d), we can see that the ablation depth increases dramatically while increasing the number of pulses. In addition, there is a slight increase of the crater diameter. Figure 6 shows three simulated 3D ablation craters with a fixed number of pulses $N = 500$ and laser fluence $F = 2.3\,J/cm^2$ but different laser beam waists: $w_0 = 4.5$, 8.5, and 12.4 μm. The cross-sectional profiles at the centerline of the craters are plotted in Fig. 6(d), in which the

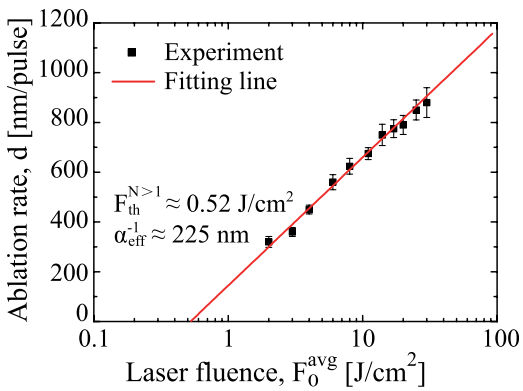

FIG. 3. Ablation rate of aluminum using laser pulse of $\lambda = 800\,nm$ and $t_p = 100$ fs. The solid lines are fitted according to Eq. (11). The slope of the linear line can be interpreted as the effective optical penetration depth α_{eff}^{-1}. The extrapolation to zero provides the multi-pulse ablation threshold $F_{th}^{N>1}$.

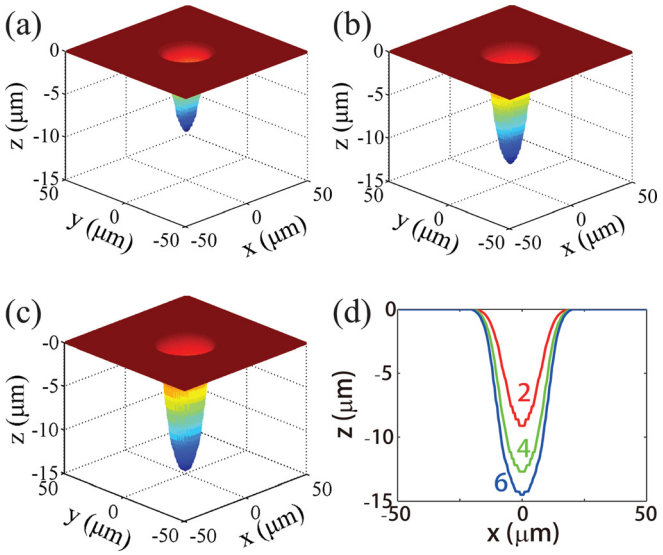

FIG. 4. Simulated 3D ablation craters by multi-pulse laser with different energy fluences. (a) $F = 2\,\mathrm{J/cm^2}$; (b) $F = 4\,\mathrm{J/cm^2}$; (c) $F = 6\,\mathrm{J/cm^2}$; (d) center-line profiles of the ablation craters.

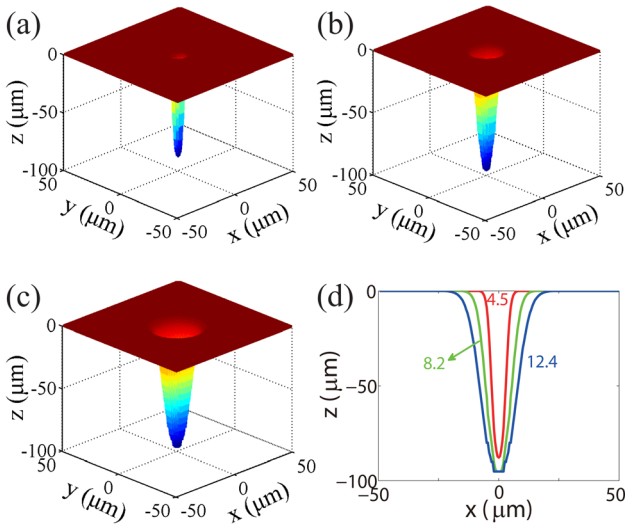

FIG. 6. Simulated 3D ablation craters by multi-pulse laser with different beam waists. (a) $w_0 = 4.5\,\mu$m; (b) $w_0 = 8.2\,\mu$m; (c) $w_0 = 12.4\,\mu$m; (d) center-line profiles of the ablation craters.

crater diameter increases linearly with the increase of laser beam waist w_0, while the depth of craters remains stationary by varying beam waist w_0. In conclusion, both the laser fluence and the number of pulses mainly affect the crater depth, while the beam waist is a dominant parameter that affects the crater diameter.

Figure 7 demonstrates that the number of pulses for drilling-through a 100-μm-thick aluminum plate sample is a function of the laser fluence in our simulation and experiment. The laser fluence starts from the multi-pulse ablation threshold $F_{th}^{N>1} = 0.52 \pm 0.01\,\mathrm{J/cm^2}$. During the ablation process, the transmission light mounted under the aluminum film can not be recorded by the CCD unless the film was drilled through. In other words, the number of pulses going through the aluminum film was defined as the time from the beginning of ablation to the appearance of transmission light on the CCD camera. The drilling-through time can be recorded by a beam shutter and an average datum of five measurements was used for each point in the experiment. As illustrated in Fig. 7, the simulation and experimental curves are in good agreement. The number of pulses for drilling through declines dramatically along with the increase of the laser fluence until it reaches point A at $F = 1.2\,\mathrm{J/cm^2}$, and varies slowly since then. Point A is considered as a saturation point of the ablation, which is due to the plasma shield effect. Since it is neglected in the two-temperature model, the same point A cannot be seen in simulation results.

We further confirm the relationship between the hole shape (a ratio of depth/entrance hole diameter) and the laser fluence. When changing the number of pulses, hole forming process was simulated under the laser fluences of 1 and $3\,\mathrm{J/cm^2}$. The number of the laser pulses was set from 100 to 1600 shots per hole. The hole depth and the entrance hole diameter were measured, respectively. We calculated the relationship between the ratio of depth/entrance hole diameter

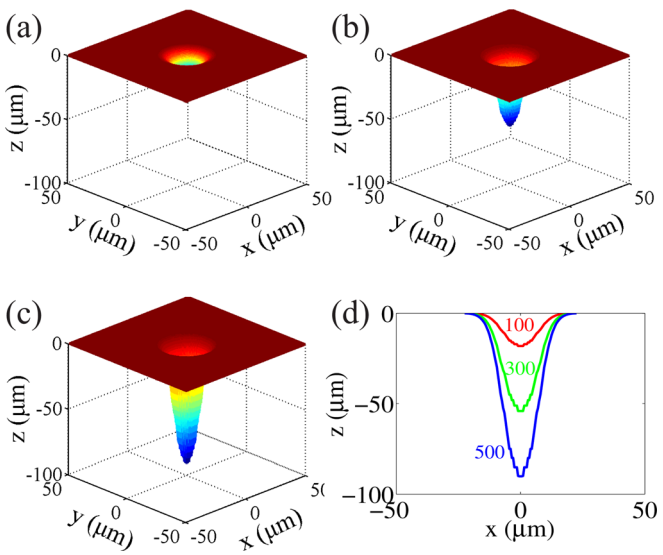

FIG. 5. Simulated 3D ablation craters by multi-pulse laser with different numbers of pulses. (a) $N = 100$; (b) $N = 300$; (c) $N = 500$; (d) center-line profiles of the ablation craters.

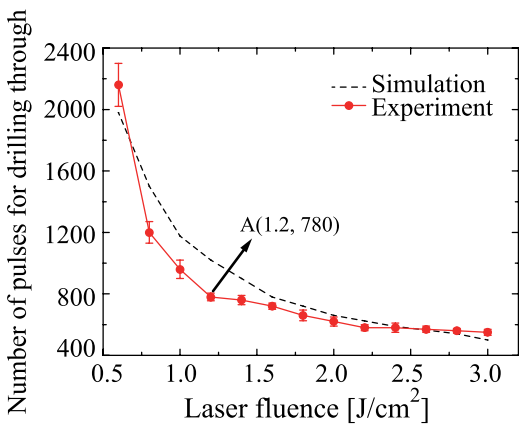

FIG. 7. Number of pulses as a function of pulse laser fluence for drilling-through a 100-μm-thick aluminum plate samples in the simulation and experiment.

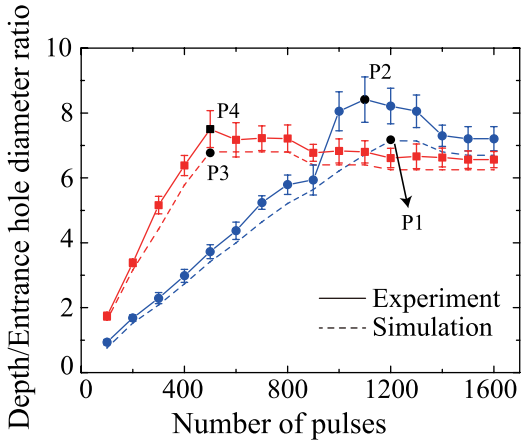

FIG. 8. Relationship between the ratio of depth/entrance hole diameter and the number of laser pulses per hole. Simulation depth/entrance diameters as a function of number of pulses for different laser fluences of $F = 1\,\mathrm{J/cm^2}$ (blue dashed line) and $F = 3\,\mathrm{J/cm^2}$ (red dashed line). The blue and red solid lines represent the corresponding experimental results, respectively.

and the number of laser pulses per hole, as shown in Fig. 8. The curves of the experiment results are in good agreement with the simulations. We also find that when the number of pulses is more than 1200 (P1), the ratio of depth/entrance hole diameter does not increase any more, where the saturation points are appeared with different laser fluences, marked as P2–4 in Fig. 8, respectively.

IV. CONCLUSIONS

In this article, an improved 3D two-temperature model was proposed and employed to simulate multi-pulse ablation of the thick metal sample. By employing it, an multi-pulse ablation threshold $F_{th}^{N>1} = 0.52 \pm 0.01\,\mathrm{J/cm^2}$ is estimated, which is lower than the predicted single-pulse threshold due to the incubation effect that decreases the thermal damage region. In our simulations and experiments, we found that laser fluence and the number of pulses mainly affect the crater depth, while the beam waist dominantly decides the crater diameter. Moreover, one can see that the higher the laser fluence, the smaller the number of pulses required to drill through the sample. For a given ablation crater depth of the thick sample, we can use this model to find proper laser pulse parameters to achieve the drilling holes with a required high aspect ratio and high quality. This will be of great instructive significance to femtosecond ablation technology.

ACKNOWLEDGMENTS

The research was supported by the National Natural Science Foundation of China under Grant Nos. 11174204, 61125503, and 61235009, the Foundation for Development of Science and Technology of Shanghai under Grant No. 13JC1408300.

[1]B. Chichkov, C. Momma, S. Nolte, F. Von Alvensleben, and A. Tünnermann, "Femtosecond, picosecond and nanosecond laser ablation of solids," Appl. Phys. A **63**, 109–115 (1996).
[2]S. Anisimov, B. Kapeliovich, and T. PerelMan, "Electron emission from metal surfaces exposed to ultrashort laser pulses," Zh. Eksp. Teor. Fiz. **66**, 375–377 (1974).
[3]A. H. Lutey, "An improved model for nanosecond pulsed laser ablation of metals," J. Appl. Phys. **114**, 083108 (2013).
[4]K. Anoop, R. Fittipaldi, A. Rubano, X. Wang, D. Paparo, A. Vecchione, L. Marrucci, R. Bruzzese, and S. Amoruso, "Direct femtosecond laser ablation of copper with an optical vortex beam," J. Appl. Phys. **116**, 113102 (2014).
[5]M. Shaheen, J. Gagnon, and B. Fryer, "Laser ablation of iron: A comparison between femtosecond and picosecond laser pulses," J. Appl. Phys. **114**, 083110 (2013).
[6]L. Jiang and H.-L. Tsai, "Repeatable nanostructures in dielectrics by femtosecond laser pulse trains," Appl. Phys. Lett. **87**, 151104 (2005).
[7]T. Qiu, T. Juhasz, C. Suarez, W. Bron, and C. Tien, "Femtosecond laser heating of multi-layer metals II. Experiments," Int. J. Heat Mass Transfer **37**, 2799–2808 (1994).
[8]H. Lao, H. Zhu, and X. Chen, "Threshold fluence for domain reversal directly induced by femtosecond laser in lithium niobate," Appl. Phys. A **101**, 313–317 (2010).
[9]Y. Liao, Y. Ju, L. Zhang, F. He, Q. Zhang, Y. Shen, D. Chen, Y. Cheng, Z. Xu, K. Sugioka *et al.*, "Three-dimensional microfluidic channel with arbitrary length and configuration fabricated inside glass by femtosecond laser direct writing," Opt. Lett. **35**, 3225–3227 (2010).
[10]A. Chen, Y. Jiang, L. Sui, D. Ding, H. Liu, and M. Jin, "Thermal behavior of thin metal films irradiated by shaped femtosecond pulse sequences laser," Opt. Commun. **284**, 2192–2197 (2011).
[11]Y. Qi, H. Qi, A. Chen, and Z. Hu, "Improvement of aluminum drilling efficiency and precision by shaped femtosecond laser," Appl. Surf. Sci. **317**, 252–256 (2014).
[12]P. Lorazo, L. J. Lewis, and M. Meunier, "Short-pulse laser ablation of solids: From phase explosion to fragmentation," Phys. Rev. Lett. **91**, 225502 (2003).
[13]W. Roeterdink, L. Juurlink, O. Vaughan, J. Dura Diez, M. Bonn, and A. Kleyn, "Coulomb explosion in femtosecond laser ablation of Si (111)," Appl. Phys. Lett. **82**, 4190–4192 (2003).
[14]X. Wang and X. Xu, "Thermoelastic wave in metal induced by ultrafast laser pulses," J. Therm. Stresses **25**, 457–473 (2002).
[15]G. Du, F. Chen, Q. Yang, J. Si, and X. Hou, "Ultrafast temperature relaxation evolution in Au film under femtosecond laser pulses irradiation," Opt. Commun. **283**, 1869–1872 (2010).
[16]S.-S. Wellershoff, J. Hohlfeld, J. Güdde, and E. Matthias, "The role of electron–phonon coupling in femtosecond laser damage of metals," Appl. Phys. A **69**, S99–S107 (1999).
[17]S. Sonntag, J. Roth, F. Gaehler, and H.-R. Trebin, "Femtosecond laser ablation of aluminium," Appl. Surf. Sci. **255**, 9742–9744 (2009).
[18]Q. Li, H. Lao, J. Lin, Y. Chen, and X. Chen, "Study of femtosecond ablation on aluminum film with 3d two-temperature model and experimental verifications," Appl. Phys. A **105**, 125–129 (2011).
[19]J. Chen, D. Tzou, and J. Beraun, "A semiclassical two-temperature model for ultrafast laser heating," Int. J. Heat Mass Transfer **49**, 307–316 (2006).
[20]L. Jiang and H.-L. Tsai, "Modeling of ultrashort laser pulse-train processing of metal thin films," Int. J. Heat Mass Transfer **50**, 3461–3470 (2007).
[21]Y. Ren, J. Chen, and Y. Zhang, "Modeling of ultrafast phase changes in metal films induced by an ultrashort laser pulse using a semi-classical two-temperature model," Int. J. Heat Mass Transfer **55**, 1620–1627 (2012).
[22]S. Mishra and V. Yadava, "Modeling and optimization of laser beam percussion drilling of thin aluminum sheet," Opt. Laser Technol. **48**, 461–474 (2013).
[23]R. Herrmann, J. Gerlach, and E. Campbell, "Ultrashort pulse laser ablation of silicon: An MD simulation study," Appl. Phys. A **66**, 35–42 (1998).
[24]Z. Lin, L. V. Zhigilei, and V. Celli, "Electron-phonon coupling and electron heat capacity of metals under conditions of strong electron-phonon nonequilibrium," Phys. Rev. B **77**, 075133 (2008).
[25]A. A. Unal, A. Stalmashonak, G. Seifert, and H. Graener, "Ultrafast dynamics of silver nanoparticle shape transformation studied by femtosecond pulse-pair irradiation," Phys. Rev. B **79**, 115411 (2009).
[26]C.-H. Fan and J. P. Longtin, "Modeling optical breakdown in dielectrics during ultrafast laser processing," Appl. Opt. **40**, 3124–3131 (2001).
[27]N. Zhang, X. Zhu, J. Yang, X. Wang, and M. Wang, "Time-resolved shadowgraphs of material ejection in intense femtosecond laser ablation of aluminum," Phys. Rev. Lett. **99**, 167602 (2007).
[28]A. Ben-Yakar and R. L. Byer, "Femtosecond laser ablation properties of borosilicate glass," J. Appl. Phys. **96**, 5316–5323 (2004).
[29]R. Srinivasan, B. Braren, and K. G. Casey, "Nature of incubation pulses in the ultraviolet laser ablation of polymethyl methacrylate," J. Appl. Phys. **68**, 1842–1847 (1990).